Electron Beam-Assisted Conjugated Polyelectrolyte/Graphene Oxide Hybrid as a Hole Transporting Material in Organic Solar Cells

Seung-Hwan Oh[1,*], Hyun Bin Kim[1] and Jin-Mun Yun[1]

[1]*Radiation Research Division, Korea Atomic Energy Research Institute, 29 Geumgu-gil, Jeongeup, Jeollabuk-do, 56212, Republic of Korea*

Abstract - The 9-bis((6′-(N,N,N-trimethylammonium) hexyl)-2,7-fluorene)-alt-(9,9-bis(2-(2-(2-methoxyethoxy)ethoxy)ethyl)-9-fluorene)) dibromide (WPF-6-oxy-F) and graphene oxide (GO) were simply blended and irradiated with electron beam under ambient conditions. Compared to the electrical conductivity of pristine GO and WPF-6-oxy-F-GO with electron beam processing, the conductivity of WPF-6-oxy-F-GO was enhanced by about three orders of magnitude because of the effect of efficient π-π packing induced by C-N bonds between WPF-6-oxy-F and GO through the electron beam processing. The WPF-6-oxy-F-GO composite was used as a hole-transporting layer (HTL) in organic solar cells (OSCs). As a result, the efficiency of the OSCs was dramatically enhanced by ~6.72% by introducing irradiated WPF-6-oxy-F-GO as an HTL in OSCs.

Key words : Water-soluble, Conjugated polymer, Graphene oxide, Organic solar cells, Hole transporting material

INTRODUCTION

Conjugated polymer-based organic solar cells (OSCs) have the advantages of low-cost, lightweight and flexibility, which enable their mass production, large-area production and roll-to-roll process (Zhang *et al*. 2002; Hope *et al*. 2004; Brabec *et al*. 2010). For these reasons, researcher have been actively developed new active and interfacial materials to get improve efficiency in OSCs. Power conversion efficiency (PCE) is determined by open-circuit voltage (V_{oc}), short circuit-current density (J_{sc}) and fill-factor (FF) parameters. As an effort to obtain a better PCE, a charge transport layer is introduced between the electrode and the active layer to improve the efficiency of carrier transport in OSCs (Walzer *et al*. 2007). There are some charge transport materials, such as conductive polymer poly(3,4-ethylenedioxythiophene): poly(styrenesulfonate) (PEDOT:PSS) (Groenendaal *et al*. 2000; Kim *et al*. 2009) and transition metal oxides (V_2O_5, (Shrotriya *et al*. 2006; Liao *et al*. 2008; Kyaw *et al*. 2008) MoO_3 (Shrotriya *et al*. 2006; Kyaw *et al*. 2008), WO_3 (Tao *et al*. 2009) TiO_2 (Shankar *et al*. 2008), and ZnO (White *et al*. 2006)). In particular, PEDOT:PSS is widely used as a hole transporting layer (HTL) or transparent electrode in OSCs because of high conductivity and solution-processability. However, PEDOT:PSS as a HTL has several drawbacks including a highly acidic nature, hygroscopic property and inhomogeneous electrical property, so these problems are related to the ITO anode corrosion, and device stability (Jorgensen *et al*. 2008). Therefore, PEDOT:PSS should be replaced with a new hole transporting layer. Graphene has a two-dimensional (2D) structure consisting of sp^2-hybridized carbon, and it has good electrical, optical and mechanical properties. For these reasons, graphene has been applied to solar cells, supercapacitors, and fuel cells and transparent electrodes in electronic devices (Novoselov *et al*. 2004; Zhu *et al*. 2010). In particular, unlike indium tin oxide (ITO), graphene has mechanical flexibility and chemical resistivity, and has also been applied to flexible electronics (Bae *et*

* Corresponding author: Seung-Hwan Oh, Tel. +82-63-570-3055, E-mail. ohsh@kaeri.re.kr

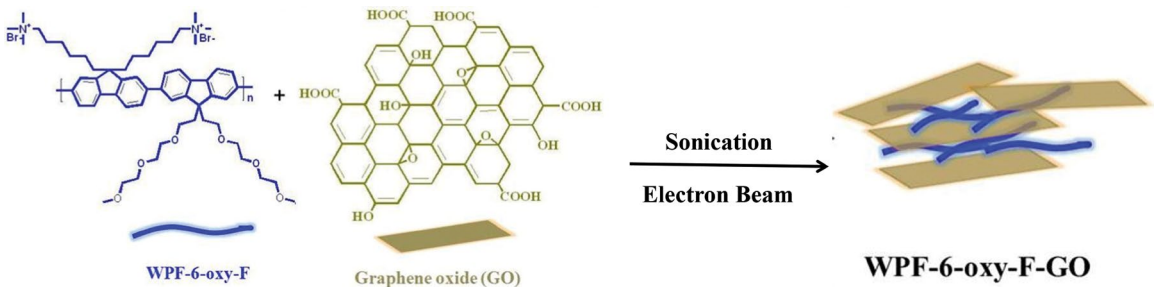

Fig. 1. The structure of the materials and the fabrication process of WPF-6-oxy-F-GO.

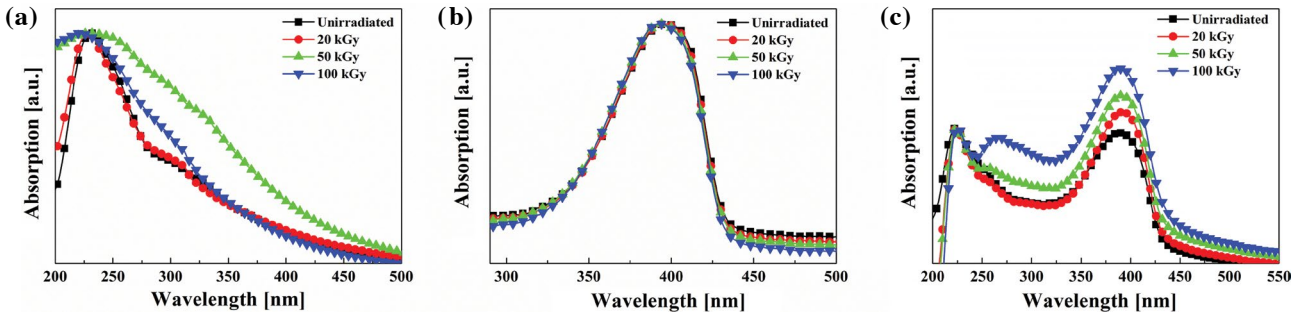

Fig. 2. UV-vis absorption spectra of (a) GO, (b) WPF-6-oxy-F and (c) WPF-6-oxy-F-GO.

al. 2010). However, the application of graphene is limited to solution-processing to fabricate flexible electronic devices because of poor solubility. Graphene oxide (GO) has emerged as an alternative to graphene. GO has high solubility and various surface modification reactions because it has a number of functional groups (carboxyl, epoxy, and hydroxyl groups) (Zheng *et al*. 2013). Even though these advantages of GO, its conductivity is lower than graphene. To enhance the conductivity of GO, reduced GO (r-GO) has generally been synthesized from GO through a chemical reduceduction method; however, r-GO experiences a low degree of dispersion in an aqueous solvent (Luo *et al*. 2011). So, it should need to development of GO with both enhanced conductivity and good dispersion at the same time to apply GO to optoelectronic devices fabricated by solution process (Li *et al*. 2010). In this study, to improve conductivity and dispersibility for solution processing, GO and water-soluble polyfluorene derivative (WPF-6-oxy-F) were simply blended and this blended solution (WPF-6-oxy-F-GO) was treated with electron beam to induce a reaction between WPF-6-oxy-F and GO. After the electron beam treatment, the conductivity of WFP-6-oxy-F-GO was improved because efficient π-π packing formed C-N bonds between the two materials by electron beam energy. This WPF-6-oxy-F-GO composite was used as a HTL between the active layer and the anode in OSCs. As a result, the PCE of the OSCs was dramatically enhanced 6.72% by introducing the WPF-6-oxy-F-GO with electron beam treatment as a HTL. Comparing WPF-6-oxy-F-GO composites with electron beam treatment and without, PCE of the WPF-6-oxy-F-GO composite with electron beam treatment was enhanced from 5.24% to 6.72%, and FF and J_{sc} also improved from 55.30% to 63.30%, 9.40 $mA \cdot cm^{-2}$ to 14.56 $mA \cdot cm^{-2}$, respectively.

MATERIALS AND METHODS

1. Preparation of the WPF-6-oxy-F-GO

The composite consisted of 9-bis((6′-(N,N,N-trimethylammonium) hexyl)-2,7-fluorene)-alt-(9,9-bis (2-(2-(2-methoxyethoxy)ethoxy)ethyl)-9-fluorene)) dibro-mide (WPF-6-oxy-F) (Oh *et al*. 2010) and graphene oxide (GO). 0.2 wt% WPF-6-oxy-F was dissolved in methanol and mixed with a 0.2 wt% GO solution in deionized water at a one-to-one ratio. The mixed solution was sonicated for 24 hours to homogeneously blend the two materials. Each blended solution was irradiated 10 kGy per scan under ambient

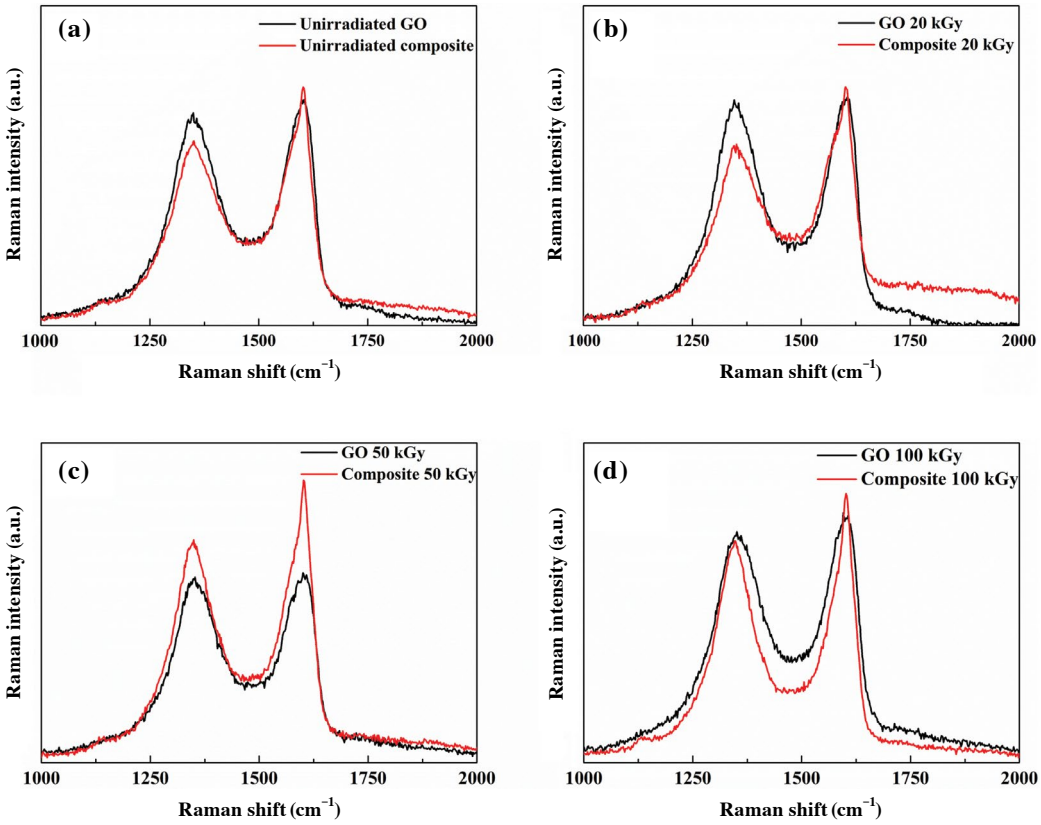

Fig. 3. Raman spectra of the GO and WPF-6-oxy-F-GO composite as a function of the electron irradiation dose with (a) 0 kGy, (b) 20 kGy, (c) 50 kGy, (d) 100 kGy.

conditions and the total irradiation doses at 20, 50 and 100 kGy, respectively.

2. Device fabrication and characterization

A patterned ITO glass (Samsung Corning Co, Ltd) with series resistance of ~10 Ω/□ was cleaned with acetone, detergent, and deionized water and 2-propanol in an ultrasonic bath. The ITO glass underwent UV-ozone treatment for 15 minutes. The WPF-6-oxy-F-GO as a HTL was spin-coated onto the ITO glass at a thickness of 3nm and annealed at 120°C for 10 min in air. A solution of 21 mg of poly((4,8-bis((2-ethylhexyl)oxy)benzo(1,2-b:4,5-b′) dithiophene-2,6-diyl) (3-fluoro-2-((2-ethylhexyl) carbonyl) thieno(3,4-b)thiophenediyl)) (PTB7, 1-material Chemscitech Inc.) and 31 mg of 1-(2-methoxycarbonly)-propyl-1-phenyl- (6,6) C_{71} butyric acid methyl-ester ($PC_{71}BM$, Nano-C) in 1.97 mL of chlorobenzene with 0.03 ml 1,8-diiodoctane was spin-coated onto the WPF-6-oxy-F-GO layer (thickness of ~70 nm) and annealed on a hot plate in a glove box at 80°C for 10 min. Ca and Al as a cathode were deposited *via* thermal evaporation with shadow mask under

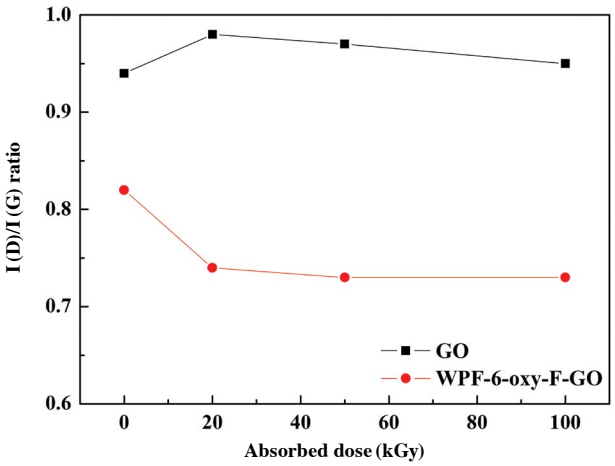

Fig. 4. I (D)/I (G) intensity ratio of GO and WPF-6-oxy-F-GO as a function of electron irradiation dose.

~10^{-7} Torr. The completed structure of the device was as follows: ITO/WPF-6-oxy-F-GO/PTB7:$PC_{71}BM$/Ca/Al. The current density-voltage (J-V) characteristics of the device was measured by Kiethly 2400 source meter under 100 mA·cm^{-2} light illumination with AM 1.5 G.

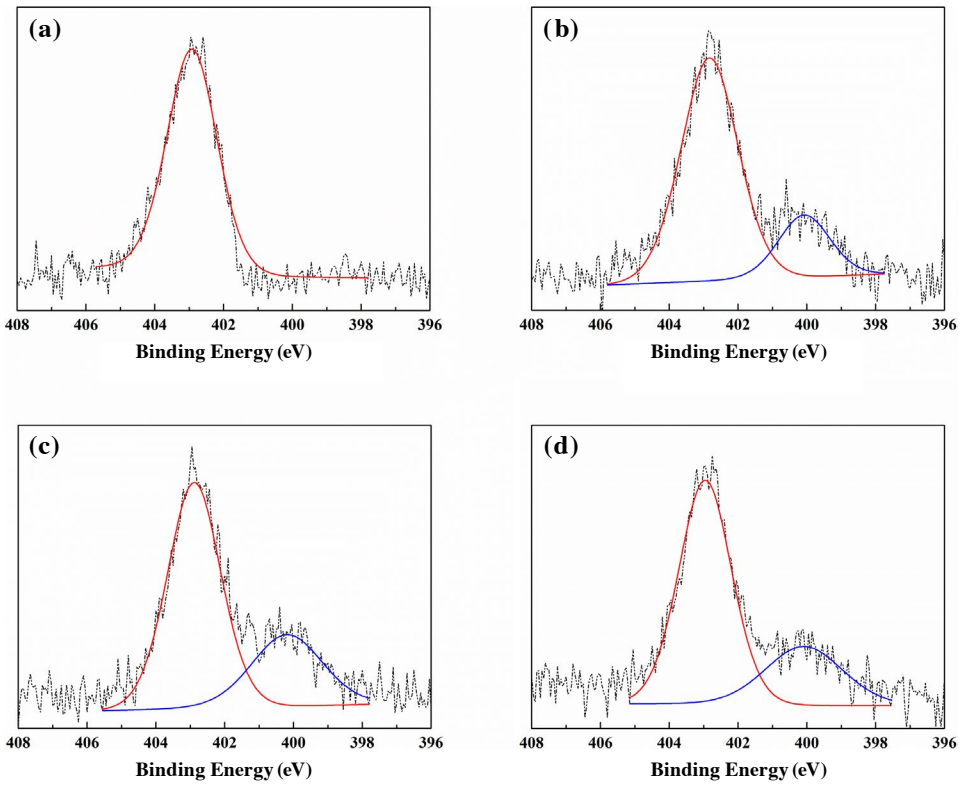

Fig. 5. N 1s XPS spectra of the WPF-6-oxy-F-GO composite as a function of the electron irradiation dose with (a) 0 kGy, (b) 20 kGy, (c) 50 kGy and (d) 100 kGy.

3. Characterization of the thin film

UV-vis absorption was measured by a Varian Cary UV-vis/NIR spectrophotometer. Raman spectra were obtained using HORIBA U1000. XPS spectra were measured by electron spectroscopy for a chemical analyzer (VG MultiLab 2000). The thin film morphologies were obtained by Veeco Dimension TM 3100. The work function and sheet resistance of the films were measured by a Kelvin probe and four-point probe (MCP-T610), respectively.

RESULT AND DISCUSSION

Fig. 1 shows the molecular structure of GO and WPF-6-oxy-F and the preparation process of WPF-6-oxy-F-GO. 0.2 wt% WPF-6oxy-F was dissolved in methanol and blended with 0.2 wt% GO in deionized water. The mixed solution was sonicated for 24 hours. The blended solution was irradiated with electron beam, and the irradiation dose was 20, 50 and 100 kGy, respectively.

UV-vis absorption spectra of the GO, WPF-6-oxy-F, and WPF-6-oxy-F-GO are shown in Fig. 2. The absorption peaks of GO and WPF-6-oxy-F-GO are shown at around 230 nm and 390 nm, respectively. The absorption peak of GO showed minor changes, and the absorption peak of WPF-6-oxy-F showed no significant change depending on increases of the electron beam irradiation dose. However, WPF-6-oxy-F-GO, absorption changed according to the radiation dose. With an increasing radiation dose, a new absorption peak appeared at a longer wavelength than the orginal absorption peak. These peaks shifted to a longer wavelength and the absorption peak intensity increased. The red-shifted absorption peaks indicate that the π-conjugated length and π-delocalization along the backbone increased (Lucht *et al*. 1998). The planar π-conjugated backbone structure of WPF-6-oxy-F enhanced the π-π interaction between GO and WPF-6-oxy-F because of their planar π-conjugated structure. To investigate the enhanced π-conjugation between the two materials after electron beam irradiation, the Raman spectroscopy of GO and WPF-6-oxy-F-GO was mesured, respectively. Raman spectroscopy has been a widely used tool for characterization of carbon material, especially π-conjugated graphitic material.

Figs. 3 and 4 show the Raman spectroscopy results and the I (D)/I (G) intensity ratio of GO and WPF-6-oxy-F-GO.

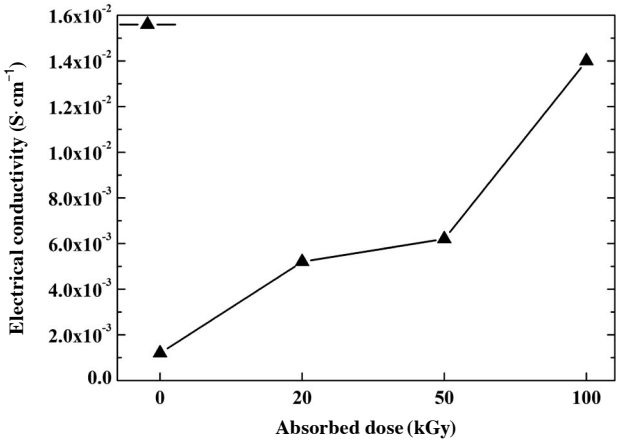

Fig. 6. The electrical conductivity of WPF-6-oxy-F-GO as a function of the electron beam irradiation dose.

As shown in the Raman spectroscopy, all samples had two notable peaks at 1350 cm^{-1} (D band) and 1600 cm^{-1} (G band). The D band located at around 1350 cm^{-1} is due to structural defects formed by the various functional groups on the carbon basal plane (Yang *et al*. 2010). The G band at around 1600 cm^{-1} is a common peak in π-conjugated graphitic materials and is attributed to the in-plane optical vibration in sp^2 carbon for π-conjugation. Unirradiated WPF-6-oxy-F-GO showed a lower D band intensity than the G band, while the D and G bands of GO indicated similar intensities.

The relative D and G band intensity (I (D)/I (G) ratio) of GO increased slightly, but there was no significant difference as the electron irradiation dose increased. However, the I (D)/I (G) ratio of WPF-6-oxy-F-GO decreased with an increase in the electron beam irradiation dose. The lower I (D)/I (G) ratio indicates decreased defects of the material because the I (D)/I (G) intensity ratio is related to the number of structural defects (Olson *et al*. 2006; Olson *et al*. 2008). The functional groups of the GO sheets reacted with the WPF-6-oxy-F, and consequently, the structural defects decreased and GO sheets became more ordered graphitized carbon with a decreasing I (D)/I (G) intensity ratio.

X-ray photoelectron spectroscopy (XPS) measurement was carried out for a detailed compositional analysis of WPF-6-oxy-F-GO. The results of the XPS measurement are shown in Fig. 5. As shown in Fig. 5, the binding energy at 402.9 eV corresponds to the ammonium salt of WPF-6-oxy-F. The N 1s spectrum of WPF-6-oxy-F shows a similar binding energy as the irradiated dose increased. When the WPF-6-oxy-F polymer was blended with GO, an additional peak is not observed except for an amine peak (~402.9 eV). However, the electron beam processed WPF-6-oxy-F-GO clearly shows a new peak at around ~400 eV, which indicated the C-N bond (Fig. 5). The new C-N bond formation was formed through the reaction between functional groups of GO and ammonium salt of WPF-6-oxy-F. The number of functional groups and defects of GO decreased because of the formation of a C-N bond, which increased the electrical conductivity and decreased the sheet resistance of WPF-6-oxy-F-GO.

Fig. 6 shows the electrical conductivity of WPF-6-oxy-F-GO as a function of electron irradiation dose. The electrical conductivity was calculated using the following equation. $\sigma = 1/(R_{sheet} \times d)$, where σ is the electrical conductivity, d is the thickness of the film, and R_{sheet} is the sheet resistance of the film. The electrical conductivity of unirradiated WPF-6-oxy-F-GO was 1.2×10^{-3} S·cm^{-1}, which is a dramatically increased value compared with GO (5.72×10^{-5} S·cm^{-1}) and WPF-6-oxy-F (1.38×10^{-7} S·cm^{-1}). In addition, the conductivity of WPF-6-oxy-F-GO continuously increased up to 1.4×10^{-2} S·cm^{-1} at 100 kGy of electron irradiation dose which is ~10^3 times higher than that of GO. Furthermore, this result is attributed to the FF and J_{sc} values in OSCs (Na *et al*. 2009), which is confirmed in Fig. 8 and Table 1. We believe that the major reason for the enhanced efficiencies of OSCs was better electrical conductivity (Cheun *et al*. 2010; Steim *et al*. 2010).

Fig. 7(a) and (b) show the device structure of OSCs and current density-voltage (J-V) characteristics curve. All the photovoltaic parameters V_{oc}, J_{sc}, FF and PCE, are summarized in Table 1. Compared to the device without the HTL, devices with electron beam processed WPF-6-oxy-F-GO showed improved photovoltaic parameters. With an increase in the irradiated dose, most of the factors improved except for V_{oc}. The V_{oc} exhibited relatively similar values in all devices because V_{oc} correlates with the highest occupied molecular orbital (HOMO) of the donor and the lowest unoccupied molecular orbital (LUMO) of the acceptor in the case of Ohmic contacts between the electrodes and the active layer with the introduction of the HTL (Steim *et al*. 2010; Yeo *et al*. 2010). The J_{sc} values of 0, 20, 50, and 100 kGy irradiated WPF-6-oxy-F-GO based-devices were 12.33, 13.91, 14.26 and 14.56 mA·cm^{-2}, which are improved values compared with an ITO only device.

The reason for the lower J_{sc} value of the ITO only device was an inefficient hole-transport from the active layer to the anode. This poor hole-transport property was also due to the high contact resistance between the active layer and the hole-

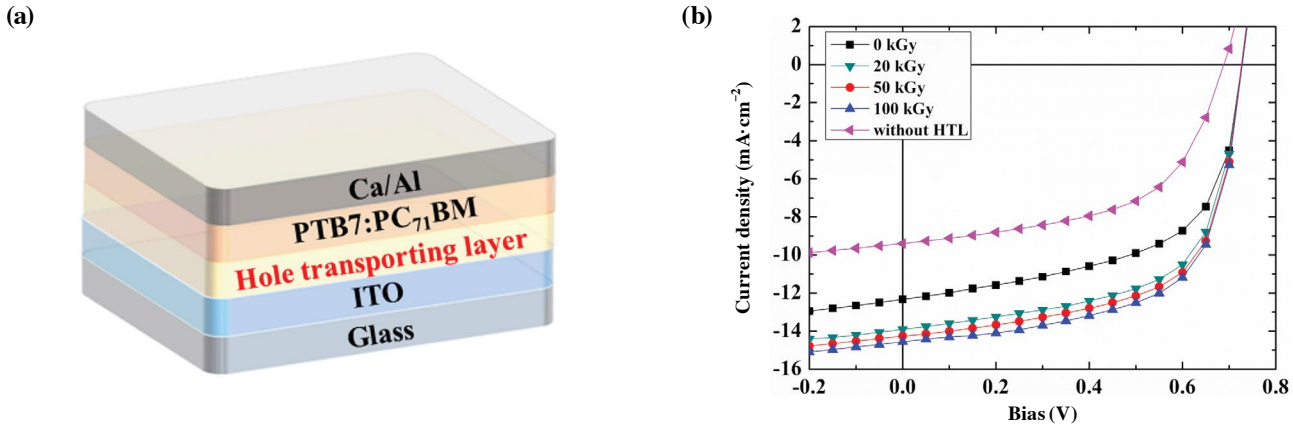

Fig. 7. (a) The device structure of OSCs with the HTL; (b) Current density-voltage (J-V) curves with and without the HTL.

Table 1. Summary of the photovoltaic parameters with the electron beam irradiation dose.

		V_{oc} (V)	J_{sc} (mA·cm^{-2})	FF (%)	PCE (%)	R_s (Ωcm^2)	R_{sh} (Ωcm^2)
WPF-6-oxy-F-GO	0 kGy	0.73	12.33	58.50	5.24	6.41	2.74E+04
	20 kGy	0.73	13.91	62.30	6.29	5.07	1.28E+06
	50 kGy	0.73	14.26	63.20	6.55	3.39	1.55E+06
	100 kGy	0.73	14.56	63.30	6.72	1.72	1.56E+06
ITO only		0.69	9.40	55.30	3.58	11.72	373.26

transporting layer. In particular, the device with 100 kGy irradiated WPF-6-oxy-F-GO showed the best performance (V_{oc} = 0.73 V, J_{sc} = 14.56 mA·cm^{-2}, FF = 63.30% and efficiency = 6.72%). The increased efficiency mainly resulted from the enhanced FF value, which is attributed to a decrease in the series resistance (R_s) and an increase in the shunt resistance (R_{sh}). R_s and R_{sh} were calculated from the slope of the J-V curve near $V = V_{oc}$ ($I = 0$) and $I = I_{sc}$ ($V = 0$), and these calculated values are listed in Table 1. By introducing electron beam irradiated WPF-6-oxy-F-GO between the anode and the active layer, R_s continuously decreased by ~1.72 Ωcm^2 because of its efficient carrier transporting property and the relatively high conductivity of film. The device with 100 kGy irradiated WPF-6-oxy-F-GO was ~10^4 times higher R_{sh} and ~10 times lower R_s compared with the device without HTL. Furthermore, an increase in the R_{sh} value means a loss of charge carriers through the leakage path (recombination or trapping of the transferring carriers to each electrode), which increased the device performance (Yip *et al*. 2008; Na *et al*. 2009).

To further investigate the morphological properties, AFM measurements were conducted. The samples for AFM were prepared by spin-coating onto a glass substrate, and the morphology was measured with a 5 μm scan size. Fig. 8(b) shows AFM images of GO and WPF-6-oxy-F-GO films with different electron beam irradiation doses. All of the AFM images show that the GO sheets were evenly spread throughout the film. In addition, the morphologies of GO showed no changes with increasing electron beam irradiation doses. However, the root mean square (rms) roughness values of the irradiated GO with 0, 20, 50, and 100 kGy was 1.16, 0.99, 0.96, and 0.93 nm, respectively. When the WPF-6-oxy-F polymer was added to GO, the GO sheets spread more widely because of the insertion of the polymer between the GO sheets. The rms roughness of GO a showed similar value, because the GO sheets had a planar structure. In comparison with the GO film only, the rms roughness of the WPF-6-oxy-F-GO films increased ~2.74 nm. The reason for the increased thickness was that the planar shaped WPF-6-oxy-F polymers were inserted into the GO sheets. The rms roughness valuse of irradiated WPF-6-oxy-F-GO with 0, 20, 50, and 100 kGy was 2.73, 4.01, 3.63, and 3.04 nm, respectively. For WPF-6-oxy-F-GO at 20 kGy of electron irradiation, the rms roughness increased ~4.11 nm, because of the interaction between the GO sheets and WPF-6-oxy-F. This interaction indicates the formation of a C-N bond, which was formed by the reaction with ammonium salt of WPF-6-oxy-F and the functional groups

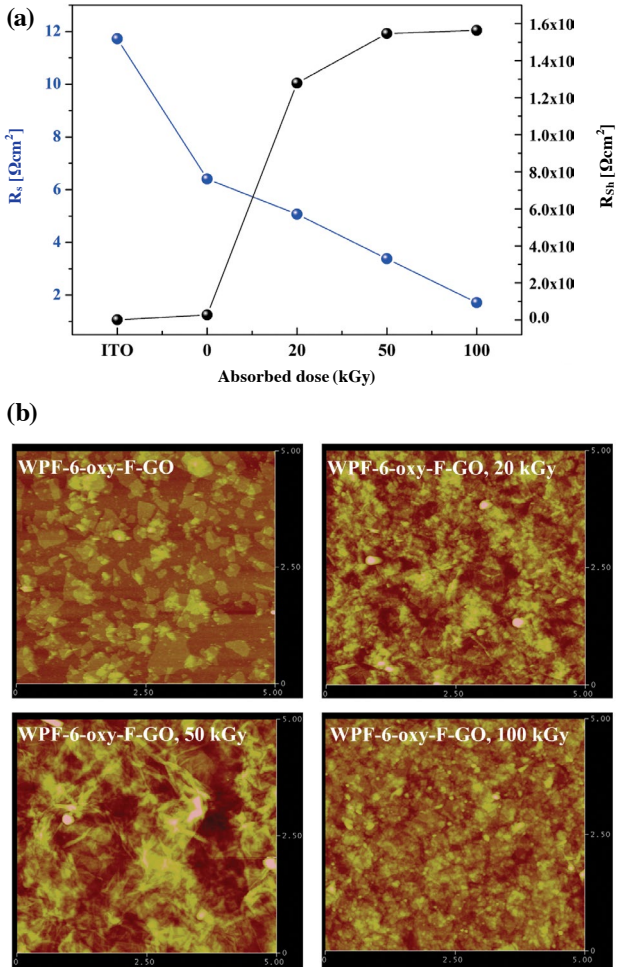

Fig. 8. (a) The R_s and R_{sh}; (b) AFM images of WPF-6-oxy-F-GO as a function of the electron beam irradiation dose.

of the GO sheets. However, for WPF-6-oxy-F-GO at 50 kGy or more, the rms roughness decreased again because of the gradually increased attraction strength between the GO sheets and WPF-6-oxy-F, which resulted from the increased number of C-N bonds.

CONCLUSION

In conclusion, we demonstrated new hole-transporting materials for OSCs. This composite material consists of a water-soluble polyfluorene derivative and GO (WPF-6-oxy-F-GO). WPF-6-oxy-F-GO was processed with an electron beam at 20, 50, and 100 kGy doses. The electrical conductivity increased with an increase in the irradiated dose. This higher conductivity enhanced the performance of the OSCs. As a result, the performance of the device with irradiated WPF-6-oxy-F-GO was enhanced up to ~6.72%. This electron beam technique could be a useful method for modifying the molecular structure and properties. In addition, a water-soluble composite WPF-6-oxy-F-GO is an attractive alternative to PEDOT:PSS as a HTL for high performance and low-cost OSCs using solution process capability.

ACKNOWLEDGMENT

This work was supported by the National Research Foundation of Korea (NRF) grant funded by the Korea Government (Ministry of Science and ICT) (NRF-2017M2A 2A6A01019867).

REFERENCES

Bae S, Kim H, Lee Y, Xu X, Park JS, Zheng Y, Balakrishnan J, Lei T, Kim H, Song YI, Kim YJ, Kim KS, Ozyilmaz B, Ahn JH, Hong B and Iijima S. 2010. Roll-to-roll production of 30-inch graphene films for transparent electrodes. *Nat. Nanotech.* **5**(8):574-578.

Brabec CJ, Gowrisanker S, Halls JJM, Laird D, Jia S and Williams SP. 2010. Polymer-fullerene bulk-heterojunction solar cells. *Adv. Mater.* **22**(34):3839-3856.

Cheun H, Hernandez CF, Zhou Y, Potscavage WJ, Kim SJ, Shim J, Dindar A and Kippelen B. 2010. Electrical and optical properties of ZnO processed by atomic layer deposition in inverted polymer solar cells. *J. Phys. Chem.* **114**(48):20713-20718.

Groenendaal L, Jonas F, Freitag D, Pielartzik H and Reynolds JR. 2000. Poly(3,4-ethylenedioxythiophene) and its derivatives: past, present, and future. *Adv. Mater.* **12**(7):481-494.

Hoppe H and Sariciftci NS. 2004. Organic solar cells: An overview. *J. Mater. Res.* **19**(7):1924-1945.

Jorgensen M, Norrman K and Krebs FC. 2008. Stability/degradation of polymer solar cells. Sol. *Energy Mater. Sol. Cells.* **92**(7):686-714.

Kim Y, Ballantyne AM, Nelson J and Bradley DD. 2009. Effects of thickness and thermal annealing of the PEDOT:PSS layer on the performance of polymer solar cells. *Org. Electron.* **10**(1):205-209.

Kyaw AKK, Sun XW, Jiang CY, Lo GQ, Zhao DW and Kwong DL. 2008. An inverted organic solar cell employing a sol-gel derived ZnO electron selective layer and thermal evaporated MoO_3 hole selective layer. *Appl. Phys. Lett.* **93**(2008):221107-221109.

Li SS, Tu KH, Lin CC, Chen CW and Chhowalla M. 2010.

Solution-processable graphene oxide as an efficient hole transport layer in polymer solar cells. *ACS Nano*. **4**(6):3169-3174.

Liao HH, Chen LM, Xu Z, Li G and Yang Y. 2008. Highly effcient inverted polymer solar cell by low temperature annealing of Cs_2CO_3 interlayer. 2008. *Appl. Phys. Lett*. **92**(2008):173303-173305.

Lucht BL, Mao SSH and Tilley TD. 1998. A zirconocene-coupling route to substituted poly(p-phenylenedienylene)s: band gap tuning via conformational control. *J. Am. Chem. Soc*. **120**(18):4354-4365.

Luo D, Zhang G, Liu J and Sun X. 2011. Evaluation criteria for reduced graphene oxide. *J. Phy. Chem. C*. **115**(23):11327-11335.

Na SI, Wang G, Kim SS, Kim TW, Oh SH, Yu BK, Lee T and Kim DY. 2009. Evolution of nanomorphology and anisotropic conductivity in solvent-modified PEDOT:PSS films for polymeric anodes of polymer solar cells. *J. Mater. Chem*. **19**(47):9045-9053.

Novoselov KS, Geim AK, Morozov SV, Jiang D, Zhang Y, Dubonos SV, Grigorieva IV and Firsov AA. 2004. Electric field effect in atomically thin carbon films. *Science*. **306**(5696):666-669.

Oh SH, Na SI, Jo J, Lim B, Vak D and Kim DY. 2010. Water-soluble polyfluorenes as an interfacial layer leading to cathode-independent high performance of organic solar cells. *Adv. Funct. Mater*. **20**(12):1977-1983.

Olson DC, Lee YJ, White MS, Kopidakis N, Shaheen SE, Ginley DS, Voigt JA and Hsu JWP. 2008. Effect of ZnO processing on the photovoltage of ZnO/poly(3-hexylthiophene) solar cells. *J. Phys. Chem. C*. **112**(26):9544-547.

Olson DC, Piris J, Collins RT, Shaheen SE and Ginley DS. 2006. Hybrid photovoltaic devices of polymer and ZnO nanofiber composites. *Thin Solid Films*. **496**(1): 26-29.

Shankar K, Mor GK, Prakasam HE, Varghese OK and Grimes GA. 2008. Effect of device geometry on the performance of TiO_2 nanotube array-organic semiconductor double heterojunction solar cells. *Journal of Non-crystalline Solids*. **354**(19-25):2767-2771.

Shrotriya V, Li G, Yao YY, Chu CW and Yang Y. 2006. Transition metal oxides as the buffer layer for polymer photovoltaic cells. *Appl. Phys. Lett*. **88**(2006):073508-073510.

Steim R, Kogler FR and Brabec CJ. 2010. Interface materials for organic solar cells. *J. Mater. Chem*. **20**(13):2499-2512.

Walzer K, Maennig B, Pfeiffer M and Leo K. 2007. Highly efficient organic devices based on electrically doped transport layers. *Chem. Rev*. **107**(4):1233-1271.

White MS, Olson DC, Shaheen SE, Kopidakis N and Ginley DS. 2006. Inverted bulk-heterojunction organic photovoltaic device using a solution-derived ZnO underlayer. *Appl. Phys. Lett*. **89**(2006):143517-143519.

Yang D, Velamakanni A, Bozoklu G, Park SJ, Stroller M, Piner RD, Stankovich S, Jung I, Field DA, Ventrice CA and Ruoff RS. 2010. The effect of chlorofluoromethanes on graphite oxidation. *Carbon*. **47**(1):145-153.

Yeo JS, Yun JM, Kim DY, Park S, Kim SS, Yoon MH, Kim TW and Na SI. 2010. Significant vertical phase separation in solvent-vapor-annealed poly(3,4-ethylenedioxythiophene):poly(styrene sulfonate) composite films leading to better conductivity and work function for high-performance indium tin oxide-free optoelectronics. *ACS Appl. Mater. Interfaces*. **4**(5):2551-2560.

Yip HL, Hau SK, Baek NS, Ma H and Jen AKY. 2008. Polymer solar cells that use self-assembled-monolayer- modified ZnO/metals as cathodes. *Adv. Mater*. **20**(12): 2376-2382.

Zhang F, Jhoansson M, Andersson MR, Hummelen JC and Inganäs O. 2002. Polymer photovoltaic cells with conducting polymer anodes. *Adv. Mater*. **14**(9):662-665.

Zheng Q, Fang G, Cheng F, Lei H, Quin P and Zhan C. 2013. Low-temperature solution-processed graphene oxide derivative hole transport layer for organic solar cells. *J. Phys. D: Appl. Phys*. **46**(2013):135101-135108.

Zhu Y, Murali S, Cai W, Li X, Suk JW, Potts JR and Ruoff JS. 2010. Graphene and graphene oxide : synthesis, properties, and applications. *Adv. Mater*. **22**(35): 3906-3924.

Received: 9 June 2019
Revised: 17 June 2019
Revision accepted: 13 July 2019